Decorrelation-based Piecewise Digital Predistortion: Operating Principle and RF Measurements

Mahmoud Abdelaziz, Lauri Anttila, Alberto Brihuega, Markus Allen, and Mikko Valkama
Department of Electrical Engineering, Tampere University, Finland
Contact email: lauri.anttila@tuni.fi

***Abstract*—In this paper, we propose a new closed-loop learning architecture for digital predistortion (DPD) with piecewise (PW) memory polynomial models. The technique is targeted specifically for power amplifiers (PAs) that exhibit strong nonlinear behavior and nonlinear memory effects, such as those implemented with gallium nitride (GaN) technology. The learning algorithm is based on a computationally simple decorrelating learning rule, which is applied on each PW polynomial model separately. Measurements with LTE-A signals on a basestation GaN PA show that the proposed technique clearly outperforms the reference closed-loop memory polynomial DPD, in terms of reducing the adjacent channel emissions.**

***Index Terms*—5G, digital predistortion, GaN power amplifiers, linearization, adaptive filters, nonlinear signal processing.**

I. Introduction

Energy efficiency is one of the key requirements in wireless communication systems, in particular when it comes to the transmitter power amplifier (PA), where much of the overall power is consumed. Gallium nitride (GaN) PA technology, for example, has proven to be an excellent choice in terms of the PA energy efficiency [1], [2]. Moreover, GaN PA devices can occupy a much smaller area for a given transmit power compared to rival technologies such as laterally diffused metal-oxide-semiconductor (LDMOS) [3]. These two advantages are quite relevant for the ongoing developments in the wireless communications industry, e.g., 5G technology and satellite communications, as well as radar.

On the other hand, efficient and compact PAs, such as GaN PAs, typically exhibit very strong nonlinear characteristics and strong nonlinear memory effects [3]–[6]. These induce in-band and out-of-band distortion to the transmit signal that can lead to violations of the error-vector magnitude (EVM) and adjacent channel leakage ratio (ACLR), that are imposed by regulatory bodies. Digital predistortion (DPD) is one of the most efficient and widely used PA linearization techniques. However, when the PA becomes highly nonlinear and incorporates strong nonlinear memory, classical DPD approaches require a significant number of parameters to be learned which leads to high complexity and possible numerical problems [7]. Moreover, polynomial models with high nonlinearity orders have poor extrapolation properties which is a disadvantage when linearizing highly nonlinear PAs [8].

Piecewise (PW) polynomial-based models have been shown to be quite effective in modeling and predistorting PAs with strong nonlinear effects [8], [9]. Moreover, the PA input/output characteristics can indeed vary over the range of the input power level thus making the modelling and predistortion a relatively difficult task when a single global model is used for the whole input amplitude range. This problem is very common in energy efficient PA architectures, e.g., Doherty and envelope tracking (ET) architectures [8]. It thus becomes more practical and efficient to use PW models for modelling and predistorting such PAs.

In this paper we introduce a novel learning algorithm for DPD with PW polynomial-based models with memory. The proposed closed-loop learning algorithm is based on a computationally simple decorrelation-based learning rule [10], which is applied to learn the PW regions separately. The DPD main path processing is also performed in parallel, for each region separately, before combining the predistorted signals at the DPD output. This simple and parallel DPD structure enables high performance implementations by exploiting the parallel computing capabilities of, e.g., field programmable gate arrays (FPGA) [11] or graphics processing units (GPU) [12]. We leave these implementation aspects for future work while focus in this paper on the DPD learning and processing algorithms. We also present practical RF measurements using a medium-power basestation GaN PA to demonstrate the effectiveness of the proposed solution.

This paper is organized as follows. Section II describes the DPD main path processing. Section III introduces the novel PW DPD solution utilizing decorrelation-based learning. Section IV reports the RF measurement results. Finally, Section V concludes the paper.

II. DPD main path processing

The DPD main path processing in this paper is based on injecting a properly filtered version of the nonlinear distortion products at the PA input with opposite phase, such that the nonlinear distortion cancels out at the PA output [13], as shown in Fig. 1. The nonlinear distortion of the PA is modeled using PW polynomial models [14], i.e, each region is modeled using a separate polynomial with memory, which we refer to in this paper as a *submodel* [9]. Accordingly, the DPD model is also a PW model with memory. In this paper, we assume the generalized memory polynomial (GMP) per submodel because of its flexibility and efficiency in modeling strong nonlinear memory effects [15], [16], though in general any other submodel can be used.

The DPD output signal $\tilde{x}(n)$, with GMP for each submodel,

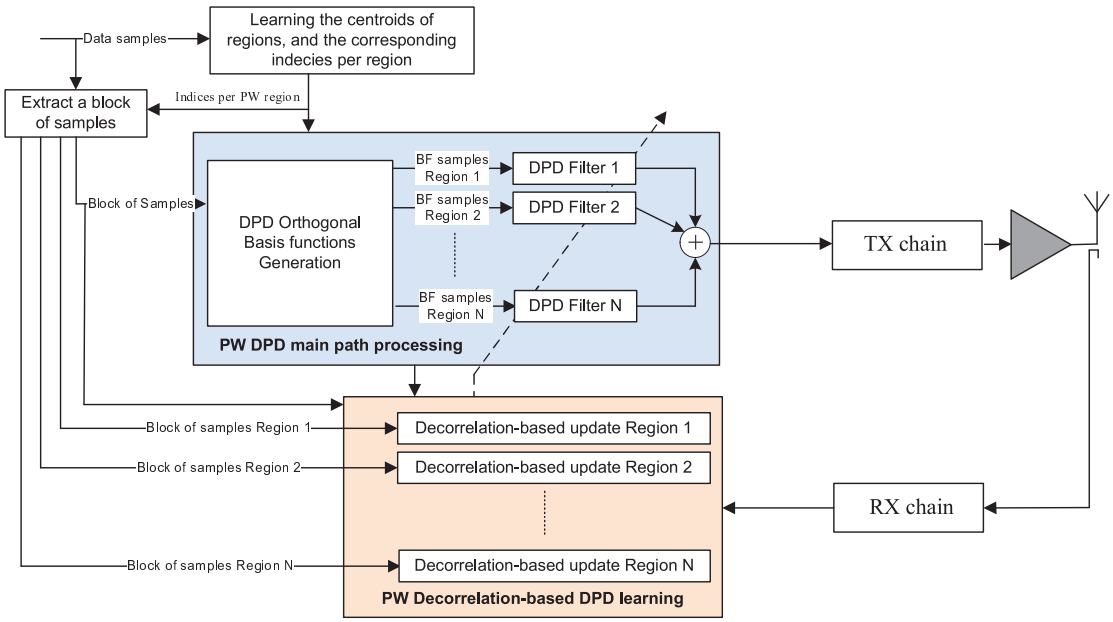

Fig. 1: Block diagram of the proposed PW DPD solution with decorrelation-based learning.

reads

$$\tilde{x}(n) = x(n) + \sum_{i=1}^{N} \sum_{\substack{p=1 \\ p \text{ odd}}}^{P} \sum_{g=-G}^{G} \alpha_{p,g,n}^{i} \star \left[|x^i(n-g)|^{p-1} x^i(n) \right] \tag{1}$$

where $x(n)$ is the complex baseband input signal, which is divided into N regions whose corresponding samples are denoted by $x^i(n)$, indicating the i^{th} region. P is the DPD nonlinearity order, G is the maximum envelope delay, and $\star$ denotes the convolution operation between the DPD filter $\alpha_{p,g,n}^{i}$ of order L, and the corresponding GMP basis function (BF) $u_{p,g}^{i}(n) = |x^i(n-g)|^{p-1} x^i(n)$. For notational convenience, each submodel is considered to have the same parameterization. However, as we also do in the experiments in Section IV, different parameterizations can be used for the different submodels. Since the basis functions $u_{p,g}^{i}(n)$ within each submodel are generally mutually correlated, the BFs can be orthogonalized by means of, e.g., Cholesky or singular value decomposition in order to improve the convergence speed and stability of the learning algorithm [14], [17]. We refer to the orthogonalized BFs as $s_{p,g}^{i}(n)$.

A successful linearization of the proposed DPD is based on proper optimization of the DPD filter coefficients per submodel $\alpha_{p,g,n}^{i}$, as well as a proper division of the baseband samples $x(n)$ into N distinct regions. These two learning aspects are addressed in the next section.

III. Proposed DPD learning

The DPD learning is divided into two separate problems. The first problem is to identify the boundaries of each region for which a separate submodel will be obtained. The second problem is the actual estimation of the DPD coefficients per submodel.

A. Learning the centroids of the PW regions

The algorithm used in this paper for partitioning the data samples into distinct regions (clusters) is known in the literature as the K-means clustering algorithm which minimizes the variance within each cluster [14]. The initial centroids (means) of the clusters are chosen randomly from the training data based on the magnitudes of the input samples. Then the following two steps are iterated until convergence:

- Each training data point is identified to the cluster whose centroid is closest to it, in the Euclidean sense
- Each centroid is then updated with the value of the new mean of the corresponding cluster.

A more efficient way to perform the clustering would consider the PA characteristics in addition to the magnitudes of the instantaneous PA input samples. We leave this to our future work.

B. Closed-loop learning of the PW-DPD coefficients

The DPD parameter optimization task is formulated such that the correlation between the nonlinear distortion at the PA output and the basis functions representing the nonlinear distortion is minimized iteratively [10]. In the proposed method, the adaptive learning is performed independently for each region. Consequently, the N adaptive DPD engines are executed in parallel, each using the data samples of the corresponding region for learning, as illustrated in Fig. 1.

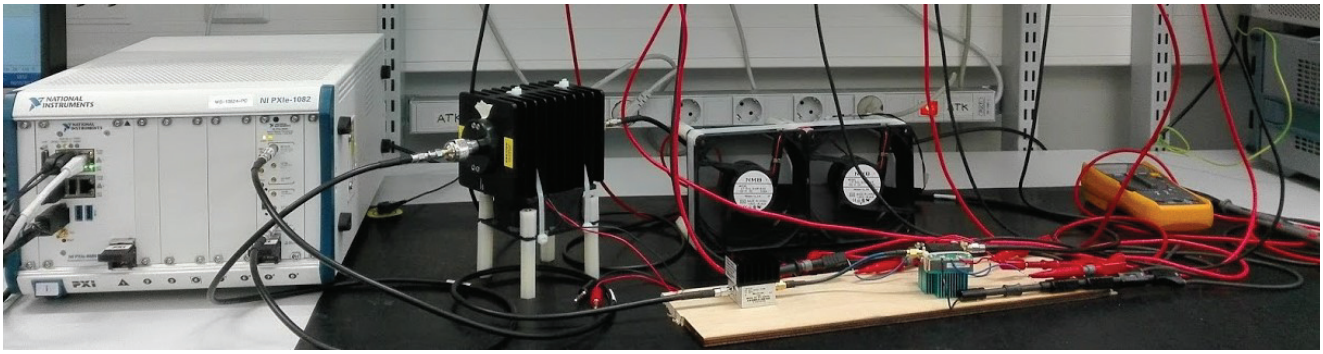

(a) RF measurement photo.

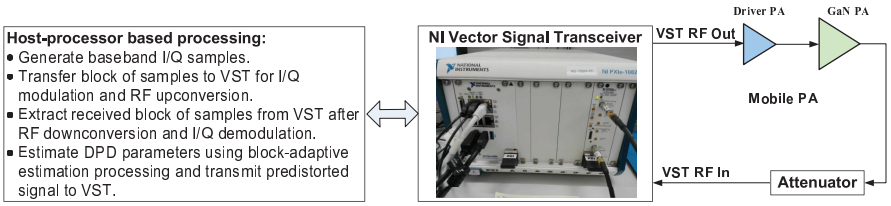

(b) RF measurement setup block diagram.

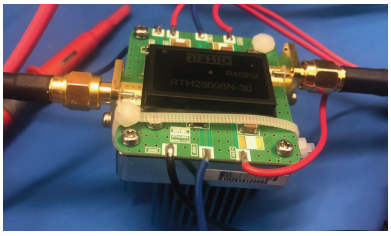

(c) GaN PA used in the measurements.

Fig. 2: RF Measurement setup and GaN PA.

Let $z(n)$ denote the baseband equivalent signal at the output of the feedback observation receiver, which captures the nonlinear distortion at the output of the PA. $z(n)$ can be thus written as

$$z(n) = F(n) \star x(n) + d(n), \tag{2}$$

where $F(n)$ is the effective linear filter, while $d(n)$ is the effective distortion due to the PA.

The error signal $e(n)$ that is used to update the DPD filter coefficients is given by

$$e(n) = \hat{F}(n) \star x(n) - z(n), \tag{3}$$

where $\hat{F}(n)$ is the estimate of $F(n)$, and it can be obtained in practice by means of, e.g., least-squares estimation.

Then, assuming a DPD filter memory order of L for each orthogonal basis function $s^i_{p,g}(n)$, and an estimation block size of M samples, we combine all the samples and the corresponding DPD filter coefficients, within processing block m, into the following vectors and matrices:

$$\mathbf{s}^i_{p,g}(n_m) = [s^i_{p,g}(n_m) \ldots s^i_{p,g}(n_m - L)], \tag{4}$$

$$\mathbf{S}^i_{p,g}(m) = [\mathbf{s}^i_{p,g}(n_m)^T \ldots \mathbf{s}^i_{p,g}(n_m + M - 1)^T]^T, \tag{5}$$

$$\begin{aligned}\mathbf{S}^i(m) = [&\mathbf{S}^i_{1,-G}(m)\, \mathbf{S}^i_{3,-G}(m) \ldots \mathbf{S}^i_{P,-G}(m) \ldots \\ &\mathbf{S}^i_{1,0}(m)\, \mathbf{S}^i_{3,0}(m) \ldots \mathbf{S}^i_{P,0}(m) \ldots \\ &\mathbf{S}^i_{1,G}(m)\, \mathbf{S}^i_{3,G}(m) \ldots \mathbf{S}^i_{P,G}(m)],\end{aligned} \tag{6}$$

$$\boldsymbol{\alpha}^i_{p,g}(m) = [\alpha^i_{p,g,0}(m)\, \alpha^i_{p,g,1}(m) \ldots \alpha^i_{p,g,L}(m)], \tag{7}$$

$$\begin{aligned}\bar{\boldsymbol{\alpha}}^i(m) = [&\boldsymbol{\alpha}^i_{1,-G}(m)\, \boldsymbol{\alpha}^i_{3,-G}(m) \ldots \boldsymbol{\alpha}^i_{P,-G}(m) \ldots \\ &\boldsymbol{\alpha}^i_{1,0}(m)\, \boldsymbol{\alpha}^i_{3,0}(m) \ldots \boldsymbol{\alpha}^i_{P,0}(m) \ldots \\ &\boldsymbol{\alpha}^i_{1,G}(m)\, \boldsymbol{\alpha}^i_{3,G}(m) \ldots \boldsymbol{\alpha}^i_{P,G}(m)]^T,\end{aligned} \tag{8}$$

where n_m denotes the index of the first sample within block m.

The block-adaptive decorrelation-based DPD coefficient update in the i^{th} region, with learning rate μ, then reads

$$\bar{\boldsymbol{\alpha}}^i(m+1) = \bar{\boldsymbol{\alpha}}^i(m) - \mu\, [\mathbf{e}^i(m)^H \mathbf{S}^i(m)]^T, \tag{9}$$

where $\mathbf{e}^i(m) = [e^i(n_m) \ \ldots \ e^i(n_m + M - 1)]^T$ and $\mathbf{S}^i(m)$ denote the error signal vector and the filter input data matrix, respectively, all within the processing block m. The updated DPD coefficients $\bar{\boldsymbol{\alpha}}^i(m+1)$ are then used to filter the next block of M samples, and the process is iterated until convergence.

IV. RF Measurement Results

In this section, RF measurement results are reported to demonstrate and validate the operation of the proposed PW-DPD solution.

A. Measurement Setup

The algorithm is tested using a medium-power basestation Doherty GaN power amplifier and compared against the classical decorrelation-based DPD from [10]. The PA (model no. RTH26008N-30) used in the measurements is designed to operate over the frequency range 2620 - 2690 MHz, with

28 dB gain and +44 dBm 1-dB compression point. Two LTE-based waveforms are considered in the RF measurements. The first one has LTE 20 MHz channel-like parameterization, that is, 1200 active subcarriers and 15 kHz subcarrier spacing, while the second waveform consists of two 20 MHz LTE-like component carriers with the same parameterizations as the first one. The subcarrier modulation is 16-QAM for both waveforms.

The National Instruments (NI) PXIe-5840 vector signal transceiver (VST) used in the RF measurements includes both a vector signal generator (VSG), and a vector signal analyzer (VSA). The I/Q samples are first generated locally on the host processor, and then transferred to the VSG to perform RF I/Q modulation at the desired power level at the PA input. The VST RF output is then connected to the input port of the GaN PA, whose output port is connected to the VST RF input through a high power attenuator, implementing the observation receiver, as illustrated in Fig. 2. The VSA performs RF I/Q demodulation and ADC to bring the signal back to digital baseband.

B. Number of DPD Filter Coefficients

In order to compare the complexity of the PW-GMP and the classical GMP DPD models, the number of model coefficients is quantified. One of the main advantages of adopting a PW solution is the fact that the parameterization of each region can be chosen differently, which allows for better optimization of the complexity-performance trade-off, by adopting simple models in the "well-behaving" regions, and more complex in those exhibiting more severe nonlinear behavior.

The number of coefficients of a GMP model is given by

$$n_{\text{Classical}}^{\text{coeff}} = (L+1) + (2G+1)(L+1)(P-1)/2 \qquad (10)$$

On the other hand, the number of coefficients of the PW-GMP is given by

$$n_{\text{PW}}^{\text{coeff}} = \sum_{i=1}^{N} (L_i+1) + (2G_i+1)(L_i+1)(P_i-1)/2, \quad (11)$$

which accounts for the different parameterization in each submodel. The total number of coefficients utilized by each DPD model are gathered in Table. II, along with the adopted GMP parameters. Four regions are utilized by the PW-GMP, as also shown in Fig. 3, and their parameters are listed by order, that is, from region one to four.

C. DPD Performance and Analysis

We now evaluate the linearization performance of both DPD solutions. The decorrelation-based learning utilizes 20 block-level iterations with 20,000 samples per block in both DPD solutions. The considered P, L and G are shown in Table II.

Fig. 4 illustrates the normalized spectra when the considered closed-loop DPD solutions are adopted, and their corresponding AM/AM responses are illustrated in Fig. 3. As it can be observed, the PW DPD solution outperforms the classical GMP DPD by a large margin, despite having comparable computational complexity.

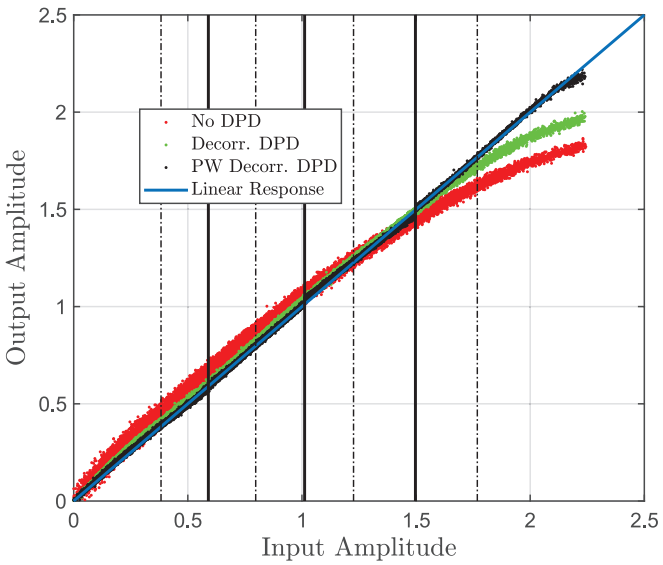

Fig. 3: RF measurement example showing the AM/AM response of the GaN PA with and without DPD at +39.5 dBm TX power. Classical decorrelation-based DPD is compared to the proposed PW decorrelation-based DPD. The region boundaries and centroids are also shown using the vertical solid and dotted lines, respectively.

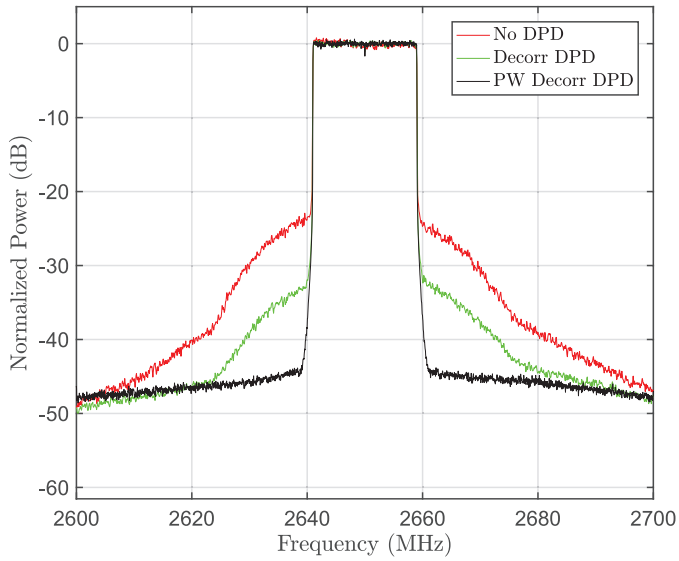

Fig. 4: RF measurement example showing the normalized spectra at the GaN PA output with and without DPD at +39.5 dBm TX power. Classical decorrelation-based DPD is compared to the proposed PW decorrelation-based DPD.

A more challenging linearization scenario is considered in Fig. 5, where an LTE-A signal with two 20 MHz component carriers is transmitted. The PW DPD solution outperforms the classical GMP again by a wide margin. The ACLR results for the two scenarios are given in Table II.

TABLE I: Parameterization and Number of Coefficients

	P	L	G	n^{coeff}
Classical GMP	11	4	3	180
Piecewise GMP	7/3/5/9	2/2/2/2	2/1/2/2	192

TABLE II: ACLR L/R results

	20 MHz signal	**40 MHz signal**
No DPD	28.46 / 29.41	28.91 / 31.67
Decorr. DPD	37.63 / 36.72	34.91 / 34.76
PW Decorr. DPD	45.24 / 44.39	42.24 / 41.35

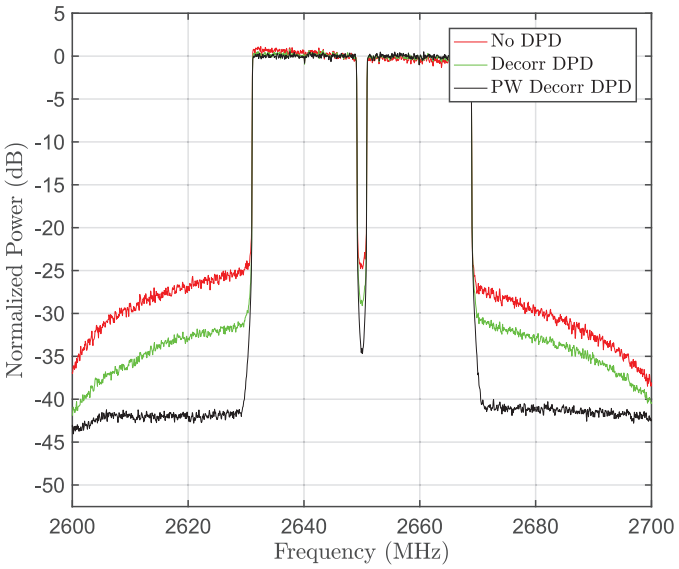

Fig. 5: RF measurement example showing the normalized spectra at the GaN PA output with and without DPD at +39.5 dBm TX power. Classical decorrelation-based DPD is compared to the proposed PW decorrelation-based DPD.

V. Conclusions

We proposed a new closed-loop learning solution for DPD with piecewise memory polynomial based models. The technique was evaluated on a basestation Doherty GaN PA with LTE-A signals in terms of the adjacent channel emissions, and was found to provide good linearization and to clearly outperform the classical GMP DPD with similar complexity. Piecewise models combined with closed-loop learning offer an effective solution for linearizing modern power-efficient and highly nonlinear PAs, such as those implemented in GaN technology.

Acknowledgments

This work was supported in part by Tekes, Nokia Bell Labs, Huawei Technologies Finland, TDK-EPCOS, Pulse Finland and Sasken Finland under the 5G TRx project, by the Academy of Finland (projects #288670 and #301820), and by TUT Graduate School.

References

[1] L. F. Eastman and U. K. Mishra, "The toughest transistor yet [GaN transistors]," *IEEE Spectrum*, vol. 39, no. 5, pp. 28–33, May 2002.

[2] U. K. Mishra, L. Shen, T. E. Kazior, and Y. Wu, "GaN-Based RF Power Devices and Amplifiers," *Proceedings of the IEEE*, vol. 96, no. 2, pp. 287–305, Feb 2008.

[3] O. Hammi and F. M. Ghannouchi, "Comparative study of recent advances in power amplification devices and circuits for wireless communication infrastructure," in *2009 16th IEEE International Conference on Electronics, Circuits and Systems - (ICECS 2009)*, Dec 2009, pp. 379–382.

[4] O. Jardel, F. De Groote, T. Reveyrand, J. Jacquet, C. Charbonniaud, J. Teyssier, D. Floriot, and R. Quere, "An Electrothermal Model for AlGaN/GaN Power HEMTs Including Trapping Effects to Improve Large-Signal Simulation Results on High VSWR," *IEEE Transactions on Microwave Theory and Techniques*, vol. 55, no. 12, pp. 2660–2669, Dec 2007.

[5] J. M. Tirado, J. L. Sanchez-Rojas, and J. I. Izpura, "Trapping Effects in the Transient Response of AlGaN/GaN HEMT Devices," *IEEE Transactions on Electron Devices*, vol. 54, no. 3, pp. 410–417, March 2007.

[6] S. Amin, P. Händel, and D. Rönnow, "Digital Predistortion of Single and Concurrent Dual-Band Radio Frequency GaN Amplifiers With Strong Nonlinear Memory Effects," *IEEE Transactions on Microwave Theory and Techniques*, vol. 65, no. 7, pp. 2453–2464, July 2017.

[7] R. Raich, Hua Qian, and G. T. Zhou, "Orthogonal polynomials for power amplifier modeling and predistorter design," *IEEE Transactions on Vehicular Technology*, vol. 53, no. 5, pp. 1468–1479, Sept 2004.

[8] A. Zhu, P. J. Draxler, C. Hsia, T. J. Brazil, D. F. Kimball, and P. M. Asbeck, "Digital Predistortion for Envelope-Tracking Power Amplifiers Using Decomposed Piecewise Volterra Series," *IEEE Transactions on Microwave Theory and Techniques*, vol. 56, no. 10, pp. 2237–2247, Oct 2008.

[9] S. Afsardoost, T. Eriksson, and C. Fager, "Digital Predistortion Using a Vector-Switched Model," *IEEE Transactions on Microwave Theory and Techniques*, vol. 60, no. 4, pp. 1166–1174, April 2012.

[10] M. Abdelaziz, L. Anttila, A. Kiayani, and M. Valkama, "Decorrelation-Based Concurrent Digital Predistortion With a Single Feedback Path," *IEEE Transactions on Microwave Theory and Techniques*, vol. 66, no. 1, pp. 280–293, Jan 2018.

[11] L. Guan and A. Zhu, "Low-Cost FPGA Implementation of Volterra Series-Based Digital Predistorter for RF Power Amplifiers," *IEEE Transactions on Microwave Theory and Techniques*, vol. 58, no. 4, pp. 866–872, April 2010.

[12] K. Li, A. Ghazi, and C. Tarver et al., "Parallel Digital Predistortion Design on Mobile GPU and Embedded Multicore CPU for Mobile Transmitters," *Journal of Signal Processing Systems*, vol. 89, no. 3, pp. 417–430, Dec 2017.

[13] M. Cabarkapa, N. Neskovic, A. Neskovic, and D. Budimir, "Adaptive nonlinearity compensation technique for 4G wireless transmitters," *Electronics Letters*, vol. 48, no. 20, pp. 1308–1309, September 2012.

[14] T. Hastie, R. Tibshirani, and J. Friedman, *The Elements of Statistical Learning*, Springer Series in Statistics. Springer New York Inc., New York, NY, USA, 2001.

[15] D. R. Morgan, Z. Ma, J. Kim, M. G. Zierdt, and J. Pastalan, "A Generalized Memory Polynomial Model for Digital Predistortion of RF Power Amplifiers," *IEEE Transactions on Signal Processing*, vol. 54, no. 10, pp. 3852–3860, Oct 2006.

[16] Y. Liu, J. Zhou, W. Chen, and B. Zhou, "A Robust Augmented Complexity-Reduced Generalized Memory Polynomial for Wideband RF Power Amplifiers," *IEEE Transactions on Industrial Electronics*, vol. 61, no. 5, pp. 2389–2401, May 2014.

[17] G. H. Golub and C. F. Loan, *Matrix Computations, Third Edition*, Johns Hopkins University Press, 1996.